Photochemistry and Photobiology, 2018, 94: 69–80

Analysis of the Electronic Structure of the Special Pair of a Bacterial Photosynthetic Reaction Center by ^{13}C Photochemically Induced Dynamic Nuclear Polarization Magic-Angle Spinning NMR Using a Double-Quantum Axis

Marija Najdanova[1], Daniel Gräsing[1], A. Alia[2,3] and Jörg Matysik[*1]

[1]Institute of Analytical Chemistry, University of Leipzig, Leipzig, Germany
[2]Institute of Medical Physics and Biophysics, University of Leipzig, Leipzig, Germany
[3]Leiden Institute of Chemistry, Leiden University, Leiden, The Netherlands

Received 24 May 2017, accepted 4 July 2017, DOI: 10.1111/php.12812

ABSTRACT

The origin of the functional symmetry break in bacterial photosynthesis challenges since several decades. Although structurally very similar, the two branches of cofactors in the reaction center (RC) protein complex act very differently. Upon photochemical excitation, an electron is transported along one branch, while the other remains inactive. Photochemically induced dynamic nuclear polarization (photo-CIDNP) magic-angle spinning (MAS) ^{13}C NMR revealed that the two bacteriochlorophyll cofactors forming the "Special Pair" donor dimer are already well distinguished in the electronic ground state. These previous studies are relying solely on ^{13}C-^{13}C correlation experiments as radio-frequency-driven recoupling (RFDR) and dipolar-assisted rotational resonance (DARR). Obviously, the chemical-shift assignment is difficult in a dimer of tetrapyrrole macrocycles, having eight pyrrole rings of similar chemical shifts. To overcome this problem, an INADEQUATE type of experiment using a POST C7 symmetry-based approach is applied to selectively isotope-labeled bacterial RC of *Rhodobacter (R.) sphaeroides* wild type (WT). We, therefore, were able to distinguish unresolved sites of the macromolecular dimer. The obtained chemical-shift pattern is in-line with a concentric assembly of negative charge within the common center of the Special Pair supermolecule in the electronic ground state.

INTRODUCTION

In photosynthesis, organisms including plants, algae and certain bacteria utilize the energy from the sun to produce from basic inorganic molecules, as water and CO_2, low-entropy organic structures. In the initial step, specialized light-absorbing pigments within the reaction center (RC) proteins absorb the light energy which will be subsequently converted into chemical energy (1,2). The photosynthetic apparatus of the purple bacterium *Rhodobacter (R.) sphaeroides* represents a "pheophytin–quinone" type of RC, also referred to as "type II" (for reviews, see Ref. 3,4).

*Corresponding author email: joerg.matysik@uni-leipzig.de (Jörg Matysik)

Ingrained in the photosynthetic membrane, the protein–pigment complex of the RC of *R. sphaeroides* is built up by the three polypeptide subunits, namely the subunits L (light weight) and the M (medium weight), providing a hydrophobic environment through their amino acid residues, and the H (heavy weight), which is mainly positioned on the cytoplasmic side of the membrane (5,6) (Fig. 1A). The subunits L and M carry the active cofactors allowing for the light-induced charge separation and electron transfer across the membrane. The cofactors in wild-type (WT) RCs include the following: a bacteriochlorophyll *a* dimer, which is referred to as the Special Pair "P" and comprising two tightly coupled bacteriochlorophylls P_L and P_M, two monomeric accessory bacteriochlorophylls *a* (B_A and B_B), two bacteriopheophytin *a* molecules (Φ_A and Φ_B), two ubiquinones (Q_A and Q_B), a carotenoid and a nonheme iron (Fe^{2+}) (Fig. 1A). The photosynthetically active cofactors are arranged in two highly symmetric branches (identified as branch "A" and "B") along a pseudo two-fold (pseudo C_2) symmetry axis normal to the membrane plane (7). The branch "A" being the "active branch" allows for electron transfer, whereas the branch "B" does not participate in the electron transfer. Hence, despite the similarity in the structure, both branches are functionally entirely asymmetric.

The functional characteristics of this purple bacterial RC have been extensively studied by various spectroscopic methods (8–14). Upon light exposure, the primary donor P gets excited into a singlet-excited state P*, from where the electron transfer chain is initiated (Fig. 1B). Within approximately 200 ps, an electron is transferred from the excited primary donor P* through the primary and secondary electron acceptor, the accessory bacteriochlorophyll *a* (B_A) and the bacteriopheophytin *a* (Φ_A), respectively, reaching the terminal electron acceptors Q_A and, if present, finally Q_B in ~200 μs (15,16). Bound to the M subunit, a carotenoid molecule (Car) is located close to the donor, breaking the structural symmetry. This carotenoid cofactor is responsible for the more rapid decay of the molecular donor triplet state (see below) and, additionally, it is relevant for photo-protection and light-harvesting (17). A general scheme on kinetics and energetics of the active cofactors is given in (Fig. 1B). In quinone-depleted or quinone-reduced preparations of bacterial RCs, as in the present report, the electron forward transfer from Φ_A to Q_A is blocked, thus, the transient spin-correlated radical pair (SCRP)

formed by a radical-cation state of the Special Pair (P^+) and a radical anion state on the electron acceptor cofactor (Φ^-), decays by electron back transfer to an electronic ground state following the singlet recombination pathway or the excited state of the donor, forming a molecular donor triplet state ^3P.

As photosynthetic SCRPs cause *photochemically induced dynamic nuclear polarization* (photo-CIDNP), NMR studies provide direct access to the electronic structure of the Special Pair on the atomic resolution. This form of light-induced non-Boltzmann nuclear spin-hyperpolarization (Fig. 2) allows for dramatic enhancement of NMR signals from the nuclei involved in the formation of the SCRP. The exact mechanism of the production of transient hyperpolarization (Fig. 3, for review see Ref. 18–21) has been proposed to be due to solid-state spin-dynamical mechanisms called three-spin mixing (22) and differential decay (23) which occur on the basis of the classical radical-pair mechanism (24,25). Practically, quinone-blocked RCs under illumination show the solid-state photo-CIDNP effect in the magic-angle spinning (MAS) NMR experiment (26–28). The high sensitivity and selectivity of the photo-CIDNP MAS NMR experiment provide an excellent analytical tool for studying photosynthetic SCRPs in great detail (29,30). This method has been applied to various photosynthetic systems (31–34).

Analysis of the RCs of *R. sphaeroides*, employing photo-CIDNP MAS NMR, has demonstrated that the origin of the functional symmetry break is not due to the acceptor (35) but that the electronic structure is already broken in the "dark" ground-state electronic structure (36–38). Also in the radical-pair state, the electron spin density is asymmetrically distributed over the Special Pair (38), an observation well in-line with previous ^{1}H-ENDOR studies (39). The asymmetry in electron spin density is caused by conformational differences of the side chains of the

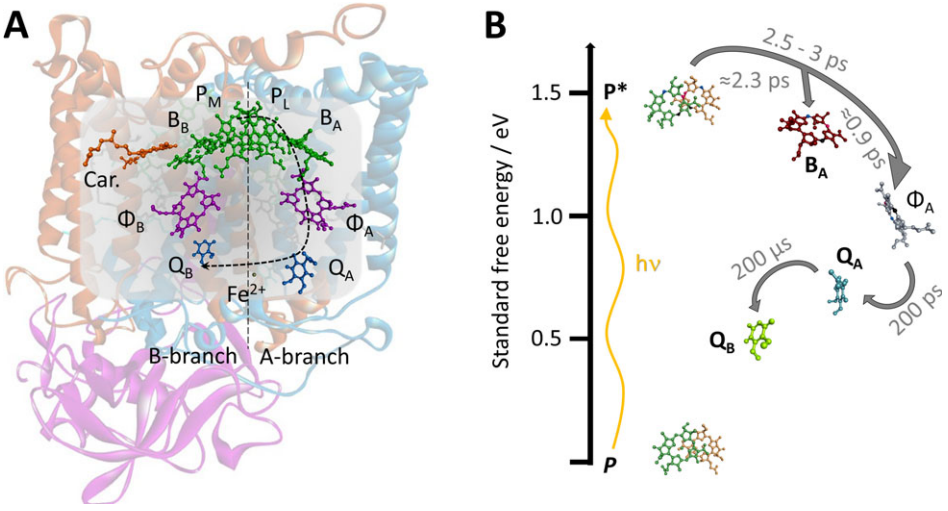

Figure 1. (A) The transmembrane bacterial RC protein complex is comprising the protein three subunits, H-heavy (purple), L-light (blue), and M-medium (orange) as well as several cofactors (5): P—bacteriochlorophyll *a* dimer (Special Pair) which upon light exposure becomes excited from the electronic ground state into the electronically excited state (P*), allowing P to act as the primary electron donor. B_A—accessory bacteriochlorophyll *a*; Φ_A—bacteriopheophytin *a*; Q_A—quinone A, and Q_B—terminal electron accepting quinone B. For details, see text. The long phytol side chains are omitted for purpose of clarity. The light-induced electron transfer is indicated by a dashed arrow [pdb entry 1M3X; the figure was prepared with Accelrys Discovery Studio, San Diego, CA]. (B) Kinetics and energetics of the stepwise electron transfer in the RC of purple bacteria (89,90). Energy excitation and kinetics for the electron transfer of the electron transfer reaction are given for each step.

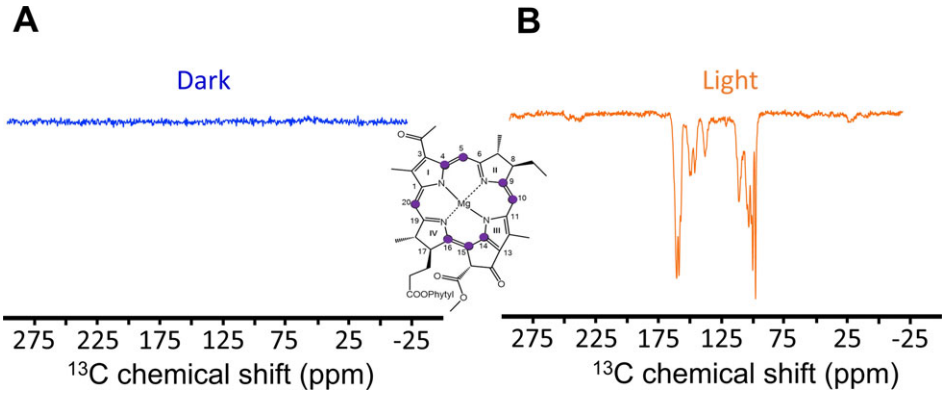

Figure 2. ^{13}C MAS NMR spectra of a bacterial RC sample obtained with selectively ^{13}C-enrichment (see offset) by feeding [5-^{13}C]-δ-aminolevulinic acid during the growth of *Rhodobacter sphaeroides* WT. The spectra have been obtained at magnetic field strength of 9.4 T, a MAS spinning frequency of 8 kHz and a temperature of 253 K. Both spectra have been obtained in <6 h each. (A) The MAS NMR spectrum taken in the dark shows virtually no signal. (B) Upon illumination with continuous white light, the photo-CIDNP spectrum occurs, exhibiting strong emissive light-induced signals as a result of the solid-state photo-CIDNP effect. The observed emissive phase of the photo-induced signals under these experimental conditions has been explained as an emissive TSM contribution overruling the enhanced absorptive DD contribution (76).

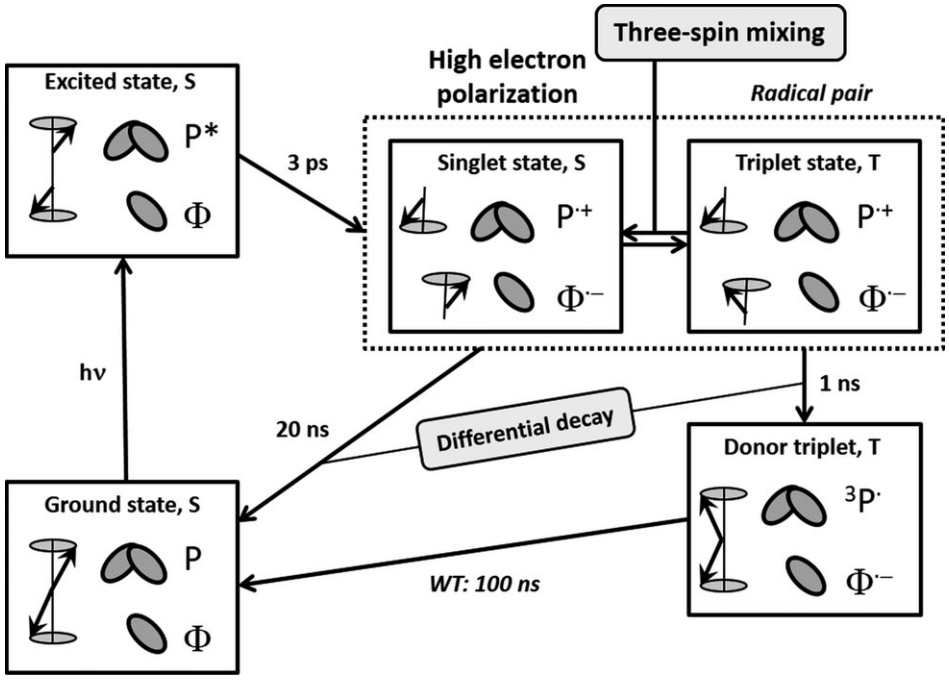

Figure 3. Mechanism of the electron transport in the quinone-blocked photosynthetic RC of *Rhodobacter sphaeroides* WT. Following light-absorption, an electron transfer step takes place from the photochemically excited state of the Special Pair (P) primary donor to the primary electron acceptor, the bacteriopheophytin of the active branch (Φ). A radical pair is born in its pure singlet state $^1(P^{\bullet+}\Phi^{\bullet-})$. The combined action of hyperfine interactions, electron Zeeman frequency difference and electron–electron coupling, controls the evolution of the spin-correlated radical pair (SCRP). During singlet-triplet interconversion, the created coherence between the electrons is transferred to the nuclei by the three-spin mixing mechanism (TSM) creating transient nuclear spin polarization. The selective decay of the SCRP also produces nuclear polarization by the differential relaxation mechanism (DD). Both mechanisms produce *net* nuclear spin-hyperpolarization, which occurs in the NMR spectrum as strong signal enhancement. Back transfer of an electron allows the system to return into the electronic ground state. A transient donor triplet state (^{3}P) is quickly relaxed by the near-by carotenoid cofactor.

tetrapyrrole macrocycles induced by different protein environments (40,41). The electronic asymmetry also occurs in the excited state (21) contributing to the selective electron transfer into only one of the two cofactor branches.

To study the electronic structure of the cofactors forming the SCRP, unequivocal chemical-shift assignment is required. To this end, the combination of two strategies, both enhancing sensitivity and selectivity, is required: ^{13}C photo-CIDNP MAS NMR as well as selective isotope labeling (36). The latter is achieved by feeding a selectively isotope-labeled precursor, δ-aminolevulinic acid (ALA), which is the first compound in the physiological porphyrin synthesis pathway. As NMR pulse scheme, homonuclear ^{13}C-^{13}C correlation experiments, as radio-frequency-driven recoupling (RFDR, see Ref. 42–44) and dipolar-assisted rotational resonance (DARR, see Ref. 35,41,45), have been adapted to the photo-CIDNP experiment by removal of the initial cross-polarization (CP) step. The removed CP step is primarily used as a strategy to enhance the sensitivity of low-gamma nuclei by transferring proton polarization. However, because of the solid-state photo-CIDNP phenomenon, a strong ^{13}C nuclear polarization is readily created and a ^{1}H-^{13}C CP transfer would only destroy this carbon hyperpolarization.

This strategy allowed to assign the majority of the ^{13}C nuclei of the Special Pair (35–37,41,46) and provided clear evidence that same carbon positions in P_L and P_M have chemical-shift differences up to 9 ppm at C-4 (37). The exact assignment of all carbons, however, is hampered by the fact, that the three macrocycles, all composed by four pyrrole rings, lead to similar sets of chemical shifts. Furthermore, the presence of yet another set of weak signals originating from a third bacteriochlorophyll (BChl) cofactor has been reported (36,37), which imposes additional challenge for the unambiguous resonance assignment. In addition, such homonuclear correlation experiments are time-consuming, as they require sampling of several mixing times to establish the macrocycle connectivities and furthermore long experimental times might additionally lead to photo-degradation.

In an attempt to obtain a conclusive assignment, we here adapt and apply a solid-state analog of a well-known liquid-state NMR experiment, the INADEQUATE pulse scheme (47–49). The ^{13}C-^{13}C homonuclear correlations can be accurately measured based on dipolar-mediated double-quantum (DQ) coherence in a 2D DQ-SQ (double-quantum single-quantum) correlation experiment (dipolar-INADEQUATE). By utilizing a DQ axis instead of a second chemical-shift axis, dipolar-generated DQ coherences (given in the indirect dimension) can be correlated to the specific isotropic chemical shifts of the macrocycle (in the direct dimension) (50–52). Ambiguities in the signal assignment of carbon connectivities, caused by spectral overlap or frequency degeneracy, can therefore be resolved by a DQ-SQ symmetry-based homonuclear dipolar-recoupling techniques, such as the 2D *permutationally offset stabilized* (POST) - C7 (50,51). Double-quantum recoupling techniques, include the two major classes of RN_n^v and CN_n^v symmetry-based recoupling schemes (52–58) as well as HORROR (53) and its modifications, have been extensively elaborated elsewhere (50,51,54–57,59). In the context of the homonuclear recoupling sequence, POST-C7, as a γ-encoding sequence with a 7-fold symmetry phase cycle, employs a phase modulation of the recoupled double-quantum Hamiltonian from the third Euler angle, giving contribution to the high DQ signal filtering efficiency in nonoriented samples

(58). With the assistance of this method, direct one-bond correlations between the isotopically enriched sites of the donor cofactor of *R. sphaeroides* WT can be revealed with a single mixing time, allowing for less crowded spectra without the signals of the isolated labeled carbons.

In this article, we present the signal assignment of the [$^{13}C_{0\text{-}8}$] selectively labeled RC of *R. sphaeroides* WT on a magnetic field of 9.4 T by utilizing a double-quantum (DQ) homonuclear dipole–dipole symmetry-based INADEQUATE approach for recoupling of the relevant interactions. The data interpretation was assisted by a newly obtained photo-CIDNP DARR MAS NMR spectrum. Hence, the photo-CIDNP INADEQUATE MAS NMR technique extends the present technology of photo-CIDNP MAS NMR by adding a method particularly suited for chemical-shift analysis of systems having many resonances with similar chemical shifts.

MATERIALS AND METHODS

Sample preparation. Rhodobacter sphaeroides WT cultures (480 mL) were grown under anaerobic conditions and in the presence of 1.0 mM isotope-labeled [5-^{13}C]-δ-aminolevulinic acid • HCl (ALA). ALA is a common precursor in the biosynthesis of tetrapyrroles. The [5-^{13}C]-ALA (99% ^{13}C enriched) was purchased from Cambridge Isotope Laboratories. The introduced pairs of isotope labels into the Special Pair and the pheophytin cofactors are given in Fig. 5C. The bacteria culture was grown under light conditions for 10 days. Subsequently, the culture was harvested and centrifuged at 5500 ***g*** over 10 min. The pallets were then combined and resuspended in 40 mL of 0.1 M phosphate buffer (pH 7.5). The RC isolation procedure has been performed as described in Ref. 60. The quinone removal was achieved by an incubation of the isolated RCs at 0.6 μM final concentration in 4% LDAO, 10 mM *o*-phenanthroline, 10 mM Tris buffer with pH 8.0 containing 0.025% LDAO and 1 mM EDTA (61). After the isolation, approximately 15 mg of [5-^{13}C]-δ-ALA-labeled RC protein (both bacteriochlorophyll (BChl) and bacteriopheophytin (BPhe) cofactors are isotopically labeled) ingrained in LDAO micelles was obtained. The isotopically labeled sample was then loaded in an optically transparent sapphire rotor for the photo-CIDNP MAS NMR measurements.

MAS NMR measurements. The photo-CIDNP MAS NMR experiments (Figs. 2 and 5) have been conducted on an Avance III NMR spectrometer (Bruker-Biospin, Karlsruhe, Germany) operating at 9.4 T, using a double-resonance MAS probe. The sample was frozen at a spinning frequency of 600 Hz in the dark, to achieve homogeneity in the sample distribution within the rotor (62). The spectra were recorded at temperature of 254 K at a MAS frequency of 8 kHz. The continuous illumination was performed as described in Ref. 28. In short, the experimental setup comprises a xenon arc lamp (1000 W; Müller Elektronik-Optik), equipped with collimation optics, a water and glass filter, focusing element and an optic fiber. The xenon lamp was chosen to provide broad light spectrum ranging between UV–Vis and near-IR. Disturbance caused by the spinning frequency counting, which is engaged by a weak light source in the near-IR region, was prevented by a water filter and by various WG320 and KG3 Schott filters. A multimode light fiber bundle, being optically transparent and providing a wide spectral range, achieves the transport of light into the desired region of the sample. The light bundle needs to be introduced through the modified MAS NMR probe in order to reach the stator so that the sample can absorb most of the illumination.

POST-C7 DQ-SQ experiment. This experiment was carried out under continuous illumination with white light at a MAS frequency of 8 kHz. The radio-frequency (RF) pulse nutation frequency for carbon was set to 56 kHz. The excitation time of the ^{13}C DQ coherence magnetization, achieved by the POST-C7 pulse sequence, was optimized to be 2.889 ms. The recovery to zero quantum (ZQ) coherence was attained by POST-C7 with the same optimized time of 2.889 ms. For excitation and reconversion of the DQ coherence, the POST-C7 symmetry-based recoupling approach was used, because it is known to be a very robust and reliable sequence which has shown very good overall performance on many different organic (biological) and inorganic materials (63–66). The continuous-wave (cw) Lee-Goldberg decoupling scheme (58,67) with 100 kHz on ^{1}H was applied during the DQ coherence excitation and the reconversion to avoid unfavorable Hartmann–Hahn matching during the recoupling. SPINAL64 decoupling scheme (68) was applied on ^{1}H with a field strength of 90 kHz during evolution of the DQ coherence and the acquisition. The SPINAL-64 decoupling under MAS has been shown to be particularly resistant toward RF inhomogeneity and pulse imperfection. In addition, it offers a satisfactory compensation of the resonance offset (69). In our experiment, the SPINAL64 showed a superior performance over TPPM for decoupling of the strong C-H dipolar interaction at moderate RF fields, for our macromolecular system. However, SPINAL64 and symmetry-based recoupling sequences interfere with each other, and therefore, continuous-wave decoupling was used to "shutdown" the C-H dipolar interactions during the DQ coherence excitation and reconversion periods.

The light-induced 2D spectra were recorded with systematic t_1 incrementation as described by Ref. 52. The pulse sequence was an adapted version of the Avance III large sweep width POST-C7 experiment in the Bruker library, and it was modified by removing the initial cross-polarization pulse for the purpose of the photo-CIDNP buildup. The read-out $\pi/2$ pulse to excite the SQ carbon coherence had a nutation frequency of 83 kHz. A recycling delay of 6 s was used. A total of 352 scans were recorded. In the t_2 dimension, 2K data points were sampled which is analogous to a spectral width of 30 kHz. Zero filling to 4K and line broadening of 20 Hz was applied prior to the Fourier transformation with a QSINE window function. In the indirect spectral dimension, 128 t_1 serial files were recorded. QSINE apodization, shifted for 90°, was applied prior to the Fourier transformation. Forward linear prediction was applied in the indirect dimension for doubling the number of acquired points. The spectrum was experimentally referenced to the ^{13}COOH signal from a tyrosine• HCl powder at 172.1 ppm.

2D ^{13}C-^{13}C photo-CIDNP dipolar-assisted rotational resonance (DARR) MAS NMR experiment. This experiment was performed on the same magnetic field strength of 9.4 T. The experiment was implemented under continuous illumination with white light, at a temperature of 254 K and a spinning frequency of 8 kHz. A spin-diffusion mixing time of 20 ms was chosen for the ^{13}C homonuclear recoupling to assure the polarization transfer within the entire macrocycle of each cofactor. A direct $\pi/2$ ^{13}C pulse with a nutation frequency of 83 kHz prepares the magnetization in the transverse plane. The magnetization is then let to evolve freely during the time t_1 where it is being modulated by the evolution frequency ω_1. Heteronuclear decoupling during the t_1-evolution is ensured by employing the SPINAL64 decoupling scheme on the ^{1}H channel with a field strength of 90 kHz (68). A second $\pi/2$ pulse aligns the magnetization along the z-axis and subsequently the mixing period begins. The efficient polarization transfer during the mixing time t_{mix} between the different ^{13}C sites is achieved via the broadened carbon transition lineshapes under the assistance of the ^{1}H-^{13}C dipolar interactions (70). During the spin-diffusion mixing period, the resonance condition $\upsilon_1 = n\upsilon_R$ (with ν_1 representing the RF pulse nutation frequency, ν_R being the MAS spinning frequency and n representing the integer matching conditions) needs to be fulfilled to reassure the heteronuclear ^{1}H-^{13}C recoupling. Hence, during the mixing period, the irradiation intensity at ^{1}H continuous-wave decoupling was optimized to fulfill the $n = 1$ rotary matching conditions (70,71). The signal was acquired under SPINAL64 decoupling on the proton channel (68). The recycling delay was 6 s. The total number of recorded scans was 352 with 1304 complex points in the t_2 and 128 real points in the t_1. The light-induced 2D DARR spectrum was acquired over a period of ~ 3 days (76 h). Zero filling to 4K and an exponential apodization of 50 Hz was applied prior to the Fourier transformation. The spectrum was experimentally referenced to the ^{13}COOH signal from a tyrosine •HCl powder at 172.1 ppm.

RESULTS AND DISCUSSION

Adaptation of a DQ-SQ POST-C7 recoupling technique for INADEQUATE photo-CIDNP MAS NMR

The through-bond correlation INADEQUATE experiment is well-known in solution-state NMR (47,48), although the

application of this technique in the solid-state is difficult because the scalar coupling is much weaker compared to the rest of the spin interactions. However, *J*-based INADEQUATE experiments have also been demonstrated in solids (72,73). Homonuclear carbon connectivities can alternatively also arise from dipolar interactions. Dipolar couplings provide long-range and through-space ^{13}C-^{13}C connectivities under solid-state conditions. Hence, dipolar-mediated DQ-SQ techniques at short mixing times are an adequate substitution for the scalar-INADEQUATE experiment as a resonance assignment method. Furthermore, this experiment permits a rapid DQ excitation so that the signal decay due to T_2 relaxation is diminished.

In MAS NMR, sample spinning removes the anisotropic dipolar interactions between adjacent ^{13}C spins, and to recover this valuable information in a nonselective (*i.e.* broadband) manner, multidimensional spin manipulating techniques are required. A large variety of ^{13}C-^{13}C broadband recoupling schemes have been developed such as RFDR (42), DREAMS (74), RIL (75), C7 (50,51). All of these recoupling schemes apply series of RF pulses, which perform transient nuclear spin recoupling, to selectively recover the desired dipolar interaction. Here, the phase-permuted POST-C7 recoupling scheme is adapted to the photo-CIDNP MAS NMR experiment by removal of the initial cross-polarization step (Fig. 4). The dipolar INADEQUATE experiment is performed under continuous illumination, to continuously produce ^{13}C hyperpolarization. The DQ excitation and the subsequent reconversion was achieved by the POST-C7 sequence (50–52). The DQ coherence is generated during the delay τ_{exe}, by the POST-C7 block composed of a train of seven subsequent RF phase alternating pulses. The formed DQ coherence evolves in the period t_1 and is modulated by the sum of the chemical-shift frequencies from the directly bond carbon pairs. The reconversion of the DQ coherence is finally performed by another POST-C7 block during the second delay τ_{rec} (51,52). The RF power applied on the recoupled spins needs to satisfy the symmetry condition $\omega_{nut}^{13C} = 7\ \omega_R$. DQ excitation, as well as reconversion is performed under LG-decoupling on the proton channel to avoid Hartmann–Hahn matching. The DQ evolution during t_1 and the signal acquisition is performed under SPINAL64 decoupling scheme. The duration of one POST-C7 sequence was adjusted in a way that a single modulation cycle corresponded to two rotor periods $\tau_R = |2\pi/\omega_R|$. This recoupling scheme is characterized by a significant DQ recoupling efficiency owing to the low orientation dependence of the averaged Hamiltonian.

Assignment of signals in the 2D photo-CIDNP INADEQUATE MAS NMR Spectrum

Figure 5A shows parts of a one-dimensional photo-CIDNP ^{13}C MAS NMR spectrum obtained with simple $\pi/2$ pulse followed by a rotor-synchronized Hahn echo to delay the FID detection (26). The spectrum shows light-induced signals from all ^{13}C labeled carbon positions including those of the isolated carbon positions C-20. The negative sign of all resonances can be attributed to the predominance of the TSM over the DD mechanism (76,77).

The 2D DQ-SQ photo-CIDNP MAS NMR spectrum of the 5-ALA-labeled RC of *R. sphaeroides* WT obtained under illumination is shown in Fig. 5B. A "dark" 1D spectrum (see Figure S1) does not show any signal in the region of interest; thus, all signals in the 2D spectrum of Fig. 5B are light-induced. The light-induced signals originate from the site-directed ^{13}C labeled positions in the electron donor cofactors (P_L and P_M) as well as the BPhe electron acceptor cofactor (Φ_A) (Fig. 5D). As each cofactor of the SCRP contains eight ^{13}C labels, a maximum of 24 signals might appear. The signals from the isolated C-20 position, however, are not expected, as they do not have a direct dipolar correlation partner. Therefore, in the 2D DQ-SQ correlation

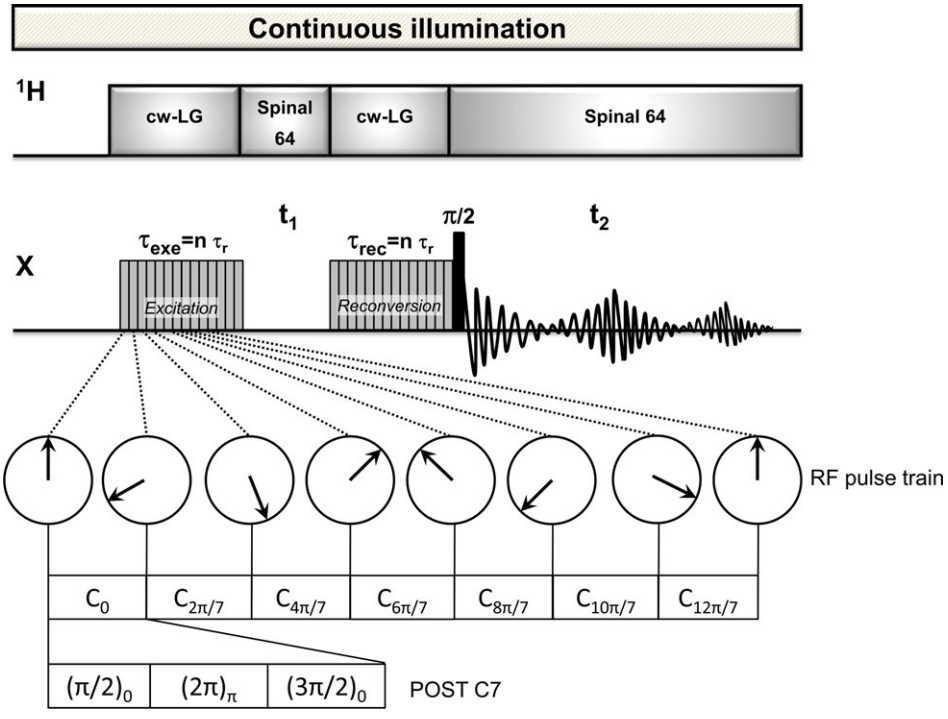

Figure 4. Pulse sequence of the 2D ^{13}C-^{13}C photo-CIDNP DQ-SQ POST-C7 MAS NMR experiments (50–52).

experiment a total of 21 carbons, originating from the three photochemically active cofactors, might contribute.

The 2D INADEQUATE photo-CIDNP MAS NMR spectrum (Fig. 5B) reveals 18 of the expected 21 signals suggesting that there is still some resonance overlap between some of the signals (37,38). We also identify 12 correlation contacts (indicated by a colored horizontal linking line). Due to the label pattern, there are three types of correlation networks: C-4 and C-5 as well as C-9 and C-10 form pairs of labels in all three cofactors. Furthermore, there is network of the three neighboring carbons C-14, C-15 and C-16.

The NMR chemical shifts of BChl *a* and BPhe *a* obtained in liquid solution in acetone-d_6 as well as in solid aggregates (Table 1) can be used for guidance for signal assignment. The chemical-shift comparison between the monomeric BChl *a* in acetone-d_6 and the BChl *a* cofactors from the RC is feasible as the coordination state of the magnesium ion in both cases is 5-coordinated (36,78,79). Also in solid BChl aggregates, the coordination number of the central magnesium is five (80). Furthermore, chemical-shift assignments based on previous homonuclear ^{13}C-^{13}C RFDR experiments (36,38,77) as well as the ^{13}C-^{13}C DARR spectrum shown in the present study (Fig. 5C) can assist for assignments.

There are some signals which appear in the 1D spectrum (Fig. 5A) but not in the 2D spectrum (Fig. 5B). The reason is that the DQ filter does not allow the isolated labeled carbons to appear. Hence, the signals which do appear in the 1D but not in the 2D spectrum (Fig. 5B) can readily be assigned to the isolated C-20 position. In fact, the emissive signals in the 2D DQ-SQ spectrum at 95.0 and 103.2 ppm can be assigned to the isolated methine carbons ^{13}C-20 from the BPhe *a* and BChl *a* cofactors. Furthermore, this assignment can be confirmed by the photo-CIDNP DARR spectrum at a mixing time of 20 ms (Fig. 5C), which reveals the appearance of the correlations for ^{13}C-20/^{13}C-4 of Φ_A at 95.0 and 137 ppm and for ^{13}C-20/^{13}C-4 of P_L at 95.0 and 136.6 ppm. A weak correlation signal at 95.0 and 157.9 ppm is also observed which can be assigned to the correlation between ^{13}C-20/^{13}C-16 of Φ_A. The ^{13}C-20 P_M methine assignment can be confirmed through the correlation peak at 103.2 and 145.1 ppm which can be assigned to the ^{13}C-20/^{13}C-4 of P_M.

The signals in the region of the SQ axis (Fig. 5B) between 90 and 110 ppm can be assigned to the enriched methine carbons (^{13}C-5; ^{13}C-10; ^{13}C-15), and this region will be the starting point for the assignment process. Correlations are observed between these methine resonance and their neighbors, namely ^{13}C-5/^{13}C-4, ^{13}C-10/^{13}C-9, ^{13}C-15/^{13}C-14 and ^{13}C-15/^{13}C-16. The signals between 130 and 166 ppm arise from these near-by aromatic pyrrole carbons. On the DQ axis, the sum of the two chemical shifts is given in ppm ($\omega_{DQ} = \omega_X + \omega_Y$, where ω_X and ω_Y represent the detected ^{13}C resonances of the directly dipolar-correlated carbon spins).

In the 2D DQ-SQ spectrum, two pairs of signals, at 97.3 and 136.6 ppm and at 101.2 and 145.1 ppm, respectively, appear more shielded in the DQ dimension compared with the rest of the light-induced signals. The emissive signal is at 97.3 ppm is intensive and has a chemical shift which is close to the chemical shift of C-5 of BChl *a* and BPhe *a* in acetone-d_6 (99.9 and 97.9 ppm) and in solid aggregates (98.9 and 96.5 ppm), respectively. The remarkable strength is observable in the 1D ^{13}C photo-CIDNP MAS NMR spectrum (Fig. 5A). The shape of the correlation signal in the 2D DQ-SQ spectrum (Fig. 5B) suggests that two carbons are resonating at frequencies close to each other. In fact, in earlier homonuclear correlation experiments, the signals ^{13}C-5 P_L and ^{13}C-5 Φ_A have been observed at 97.2 and 98.4 ppm, respectively (36,38,77). Furthermore, the signal at 97.3 ppm shows a direct dipolar correlation to a nearest-neighboring signal with similar intensity and signal shape at a resonance of 136.6 ppm. These signals have a total sum of 234 ppm in the DQ dimension and are well resolved from the rest of the photochemically induced signals. Analyzing the DARR spectrum in Fig. 5C, a strong correlation signal at 97.3 and 136.6 ppm is also detected. Additionally, the signal at 97.3 ppm shows two more correlations at ~ 145.1 and 160.9 ppm. The signal at 160.9 ppm can be assigned to a ^{13}C-9 as its chemical shift is close to that in acetone-d_6 (158.5 ppm) and in solid aggregates (157.9 ppm). This observation suggests a coherence transfer by ^{13}C spin diffusion between ^{13}C-5 and ^{13}C-9 over a distance of ~3.5 Å. At similar distance (~3.6 Å), the labeled positions ^{13}C-5 P_L/^{13}C-4 P_M (5) show a weak intramolecular correlation at 97.3 and 145.1 ppm (Fig. 5C, indicated by circle). The correlation partner of ^{13}C-5 P_L at a chemical shift of 136.6 ppm can be assigned to ^{13}C-4 P_L, whereas the partner at 160.9 ppm can be assigned to ^{13}C-9 P_L. The most shielded peak (97.3 ppm), also by considering the limited effect of ring-current shifts (76), entails to have an increased electron density, which is known to occur in the overlapping region of both pyrrole rings I of the Special Pair. Therefore, and in-line with previous studies, the signal pair of 97.3 and 136.6 ppm is safely assigned to the ^{13}C-5/^{13}C-4 pair from pyrrole ring I of P_L (20,36,37). The corresponding ^{13}C-5/^{13}C-4 pair of P_M can be assigned to the signal pair 101.2 and 145.1 ppm with a sum of 246.0 ppm in the DQ frequency. This pair of signals appears in the region very close to the expected ^{13}C-5/^{13}C-4 responses from BChl *a* in acetone-d_6 (99.9 ppm and 150.0 ppm, respectively) (37,80). The ^{13}C-5 and ^{13}C-4 resonances of Φ_A occur in solution of acetone-d_6 at 97.9 and 138.1 ppm, respectively. Hence, the correlation at 97.5 and 137.0 ppm is assigned to the ^{13}C-5/^{13}C-4 Φ_A. This signal

Figure 5. (A) 1D photo-CIDNP ^{13}C MAS NMR spectrum recorded with a Hahn-echo pulse sequence, two-pulse phase modulation (TPPM) decoupling on the proton channel and a CYCLOPS phase cycle (25). The MAS frequency was 8 kHz, and the temperature was 254 K. (B) The 2D ^{13}C-^{13}C SQ-DQ photo-CIDNP MAS NMR spectrum of selectively labeled [$^{13}C_{0\text{-}8}$] BChl/BPhe-labeled RCs from *Rhodobacter sphaeroides* WT, recorded under continuous illumination with white light at a magnetic field strength of 9.4 T, temperature of 254 K and a spinning frequency of 8 kHz. The spectrum represents a zoom into the region of interest. Chemical-shift information and assignments for the correlation pairs are provided in various colors. The full 2D spectrum is presented in the supporting information (Figure S2). (C) 2D ^{13}C-^{13}C DARR photo-CIDNP MAS NMR spectrum of selectively labeled [$^{13}C_{0\text{-}8}$] BChl/BPhe-labeled RCs from *Rhodobacter sphaeroides* WT, recorded at a magnetic field strength of 9.4 T, mixing time of 20 ms, temperature of 254 K and a spinning frequency of 8 kHz. The colored lines indicate the sequence of neighbor correlations as to confirm the chemical-shift assignments of the DQ-SQ experiment. Intramolecular long-range correlations (*i.e.* via two or three C-C bonds) are marked by the symbol ▲, whereas intermolecular correlations are indicated by encircling. (D) The ^{13}C labeled positions on the Special Pair donor BChls (P_M and P_L) and the acceptor BPhe (Φ_A) cofactor obtained upon 5-ALA labeling. Correlation pairs are indicated in color.

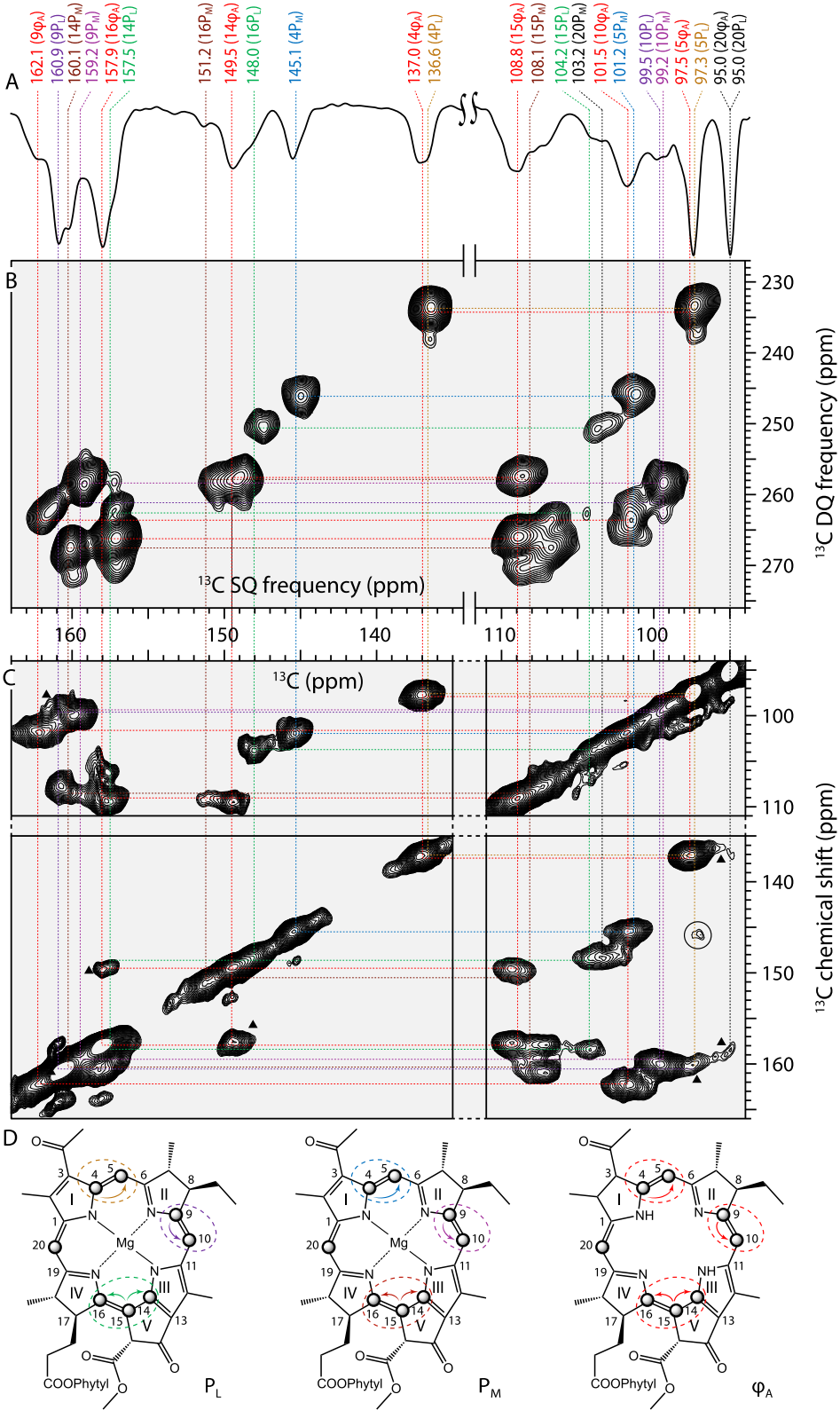

assignment is confirmed by the DARR experiment (Fig. 5C) and is in-line with previous work (37).

The next correlation pair appears at 104.2 and 148.0 ppm with a sum on the DQ frequency axis of 251.0 ppm. Having the same chemical shift of 104.2 ppm in the SQ dimension but a downfield shift on the DQ axis, a weak peak is observed with a correlation partner at 157.5 ppm (SQ frequency). Considering the labeling pattern, the peak at 104.2 ppm is assigned to a ^{13}C-

Table 1. Summary of ^{13}C chemical-shift assignment of the photo-CIDNP signals from RC of *Rhodobacter sphaeroides* WT obtained at 9.4 T.

	Chemical shifts (ppm)									
	BChl *a*						BPhe *a*			
Assign. Atom	σ_{liq}*	σ_{ss}*	$\sigma^{\dagger,\ddagger}$ (SQ) P_L	$\sigma^{\dagger}$ (DQ) P_L	$\sigma^{\dagger,\ddagger}$ (SQ) P_M	$\sigma^{\dagger}$ (DQ) P_M	σ_{liq}*	σ_{ss}*	$\sigma^{\dagger,\ddagger}$ (SQ) Φ_A	$\sigma^{\dagger}$ (DQ) Φ_A
1	151.2	153.5					139.7	136.9		
2	142.0	140.9					138.5	135.9		
3	137.7	135.7					135.0	127.1		
4	**150.0**	**151.9**	**136.6**	**234.0**	**145.1**	**246.0**	**138.1**	**135.9**	**137.0**	**234.0**
5	**99.9**	**98.9**	**97.3**		**101.2**		**97.9**	**96.5**	**97.5**	
6	168.9	170.0					172.4	168.9		
7	48.3	47.3					49.6	49.5		
8	55.8	52.9					55.4	53.0		
9	**158.5**	**157.7**	**160.9**	**261.0**	**159.2**	**258.4**	**164.3**	**162.4**	**162.1**	**263.8**
10	**102.4**	**99.7**	**99.5**		**99.2**		**100.2**	**96.7**	**101.5**	
11	149.5	147.1					139.3	135.9		
12	124.0	120.0					121.3	117.3		
13	130.6	124.1					129.2	125.5		
14	**160.8**	**160.6**	**157.5**	**262.5**	**160.1**	**268.0**	**148.7**	**145.9**	**149.5**	**258.0**
15	**109.7**	**105.8**	**104.2**	**251.0**	**108.1**	**259.0**	**110.3**	**96.7**	**108.8**	**266.8**
16	**152.0**	**150.2**	**148.0**		**151.2**		**158.7**	**158.7**	**157.9**	
17	50.5	49.6					51.4	49.5		
18	49.5	49.1					50.9	47.6		
19	167.3	168.8					171.7	171.1		
20	**96.3**	**93.9**	**95.0**	**/**	**103.2**	**/**	**97.2**	**96.1**	**95**	**/**

σ = ^{13}C chemical shift, ss = solid-state NMR, liq = liquid-state NMR, SQ = single-quantum frequency, DQ = double-quantum frequency. *Assignment according to Ref. 80; data obtained from [u-^{13}C-^{15}N] BChl *a* and [u-^{13}C-^{15}N] BPhe *a* in acetone-d_6 (σ_{liq}) and from solid aggregates (σ_{ss}). †This work. Positions given in bold are isotopically enriched in the [$^{13}C_{0\text{-}8}$] BChl/BPhe-labeled RCs from *Rhodobacter sphaeroides* WT. ‡This work. Chemical shifts observed via the 2D ^{13}C-^{13}C DARR photo-CIDNP MAS NMR experiment. Positions given in bold are isotopically enriched in the [$^{13}C_{0\text{–}8}$] BChl/BPhe-labeled RCs from *Rhodobacter sphaeroides* WT.

15 because only that methine position allows for two correlation contacts, to ^{13}C-14 and ^{13}C-16. Therefore, also the broad peak at 108.8 ppm, having two correlation partners at 149.5 ppm and 157.9 ppm, arises from a ^{13}C-15 position. Even though the direct neighbors of these two methine carbons have very close chemical shifts, they can be clearly distinguished in the DQ frequency dimension. In addition, the broad resonance at ~108.1 ppm has two correlation partners (151.2 and a broad resonance at 160.1 ppm); thus, the signal at ~108.1 ppm is also assigned to a ^{13}C-15. Assuming that the chemical shifts of the BPhe *a* cofactor from the active branch are very similar to the monomeric BPhe *a* in solution (35), we can assign the ^{13}C-15 at 108.8 ppm with the correlation partners 149.5 (^{13}C-14) and 157.9 (^{13}C-16) ppm to the bacteriopheophytin Φ_A. This signal assignment is confirmed by the DARR crosspeaks ^{13}C-15/^{13}C-14 and ^{13}C-15/^{13}C-16 at 108.8/149.5 ppm and 108.8/157.9 ppm, respectively (Fig. 5C). Furthermore, the pair of symmetric crosspeaks at 149.5/157.9 and 157.9/149.5 ppm can be correlated to a direct two-bond intramolecular correlation between ^{13}C-14/^{13}C-16 from Φ_A (indicated by symbol ▲ in Fig. 5C).

As we have seen, the signals at 104.2 and 108.1 ppm are assigned to the ^{13}C-15 methine carbons of the two Special Pair cofactors. These chemical shifts are in-line with the ^{13}C-15 resonances observed by liquid NMR in acetone-d_6 and solid aggregates, at 109.7 and 105.8 ppm, respectively (80). From the DARR spectrum, the broad methane resonance at 108.1 ppm shows a correlation to a signal at 160.1 ppm. These two signals can be assigned to the resonance pair ^{13}C-15/^{13}C-14 P_M. The signal at 151.2 ppm, exhibiting an overlap to the ^{13}C-14 Φ_A with the resonance at 149.5 ppm, can be straightforwardly assigned to the ^{13}C-16 P_M. We continue with the analysis with the ^{13}C-9/^{13}C-10 pairs. Only two candidates can be identified from spectrum 5B for the ^{13}C methine carbon C-10 (99.2 and 101.5 ppm) suggesting that again two of the light-induced signals resonate very close to each other. Due to the absence of a central metal in BPhe, the most deshielded carbon atom (at 162.1 ppm) has been assigned to ^{13}C-9 from Φ_A (37,80), and thus, the signal at 101.5 ppm is assigned to ^{13}C-10 signal of Φ_A (37). This leaves the broad signal at ~ 99.2 ppm to be assigned to ^{13}C-10 from both P_M and P_L and its coupling partners at ~ 160.0 ppm to ^{13}C-9 of both P_M and P_L. This signal assignment is supported by the DARR experiment in Fig. 5C.

The signal assignment established here with the combined dipolar INADEQUATE and DARR scheme is summarized in Table 1 and S1. We were able to solve open questions left in previous work on a 4.7 T magnetic field strength (37). The large spectral dispersion of the DQ dimension allowed for an improved separation of the photo-CIDNP signals. Hence, the ^{13}C-15 resonances of the P_L and P_M donor and Φ_A acceptor cofactors have been reassigned to the signals at 104.2, 108.1 and 108.8 ppm, respectively. Although the signals from ^{13}C-15 of P_M and Φ_A have very similar frequencies in the SQ dimension, they can be readily distinguished via their correlations on the DQ axis. Following the same principle, the almost identical frequencies of ^{13}C-14 Φ_A and ^{13}C-16 P_M have been separated in the DQ dimension. Furthermore, the light-induced responses from the overlapping ^{13}C-9 positions of the Special Pair and the ^{13}C-14 of P_M have been distinguished through their chemical-shift separation in the DQ dimension. Finally, the new assignment based on the dipolar-INADEQUATE approach allowed deciding an unresolved question: We recognized decisively that no 4th cofactor is contributing to the light-induced signals in

continuous illumination experiments as indicated earlier (36). Hence, the introduction of a DQ axis extends the toolbox of photo-CIDNP MAS NMR for analysis of SCRPs significantly. The method is in particular valuable because photo-CIDNP MAS NMR experiments require sapphire rotors and are therefore limited in the MAS frequency.

Linewidths. In the 1D spectrum (Fig. 5A), several signals are well resolved and isolated and can therefore be used for an analysis of lineshape and linewidth (full width at half maximum, FWHM). We find for the signal at 95.0 ppm a FWHM of 74 Hz. For the strongly emissive signal ^{13}C-5 P_L (97.3 ppm) and ^{13}C-4 P_L (136.6 ppm), FWHMs of 81 Hz and 82 Hz were obtained, respectively. The lineshape is more than 90% Lorentzian. That is in-line with previous experiments (35,81) concluding that the narrow line width is a strong argument for a structurally stiff and well structured cofactor arrangement along the electron transfer chain.

In the 2D experiment (Fig. 5B), the linewidths of the isolated photo-induced signals in the SQ dimension are around 100 Hz (*e.g.* for the carbons ^{13}C-5 P_L/^{13}C-4 P_L at 97.3 and 136.6 ppm and the aromatic carbon ^{13}C-5 PM at 145.1), whereas the FWHM of the rest of the aromatic carbons is around 140 Hz (for the signal at ~157.1 ppm). The slight broadening compared to the 1D experiment might be due to relaxation contributions (T_2') or the influence from the decoupling scheme (82,83).

Electronic ground state asymmetry within the Special Pair cofactors

Here, we revisited the chemical-shift assignment of the three cofactors that participate on the formation of the radical-pair $(P_LP_M)^{+\bullet}$ $\Phi_A^{-\bullet}$ using a 5-ALA ^{13}C label pattern and an INADEQUATE pulse scheme. Obviously, as recognized before (36,37), P_L and P_M are well distinguished in their electronic ground state. Combining our assignments on 5-ALA with that of 4-ALA preparations (20,36), and comparing the chemical-shift differences toward a BChl *a* molecule in acetone solution, we obtain the pattern shown in Fig. 6. The size of the spheres correlates to the magnitude of the chemical-shift difference, whereas the colors represent either an upfield shift (red), induced by increased local electron density or a downfield shift (blue).

In general, both Special Pair cofactors show significantly more shielding (red color) compared to an isolated BChl molecule demonstrating additional partial negative charge on the dimer. This ground-state electric polarization might be caused by a flux of electron density from the two axial histidines and providing a fundamental tuning to enhance electron transfer from the Special Pair (40). The increase of ground-state electron density is in particularly high in the overlapping region (both pyrrole rings I overlap). Apparently, the "π–π sandwich" stabilizes the charge surplus and probably also the hydrogen bonding between the 3^1 acetyl group (84). Interestingly, both ends of the Special Pair appear to be slightly electron depleted. Obviously, the dimer acts also in its electronic ground state as supermolecule able to condense charge in its center, while the ends and the axial histidines contribute the charge. It appears that such "condensation" of charge is particularly suited for fast, *i.e.* efficient electron transfer, and one might assume that such dimeric structure also makes it possible to buffer the changes of charge states better than an isolated molecule. Hence, the revealed electronic ground-state structure might provide a blue print for reconstruction in artificial photosynthesis. Furthermore, the increase of the conjugated area from a single to two cofactors will allow for a red shift of the first absorption maximum, increasing the spectral range accessible to these bacteria.

Hence, both donor cofactors are partially negatively charged and condense the charge in the common center, and, interestingly, both cofactors also show very similar patterns of electric polarization at the atomic resolution: While C-3 and C-4 show maximum negative charge polarization, selectively at carbons C-9, C-11, and C-13, some positive charge polarization occurs. These patterns provide an experimental key to the supermolecular orbital structure. Until now, unfortunately, theoretical efforts mainly addressed the electronic structure of the radical-cation state (85,86), probably due to a lack of empirical ground-state data.

Although two Special Pair cofactors appear as the two symmetric wings within the common dimer structure, the chemical shifts of the P_L cofactor are generally lower compared to the P_M counterpart, implying that the P_M cofactor is more shielded.

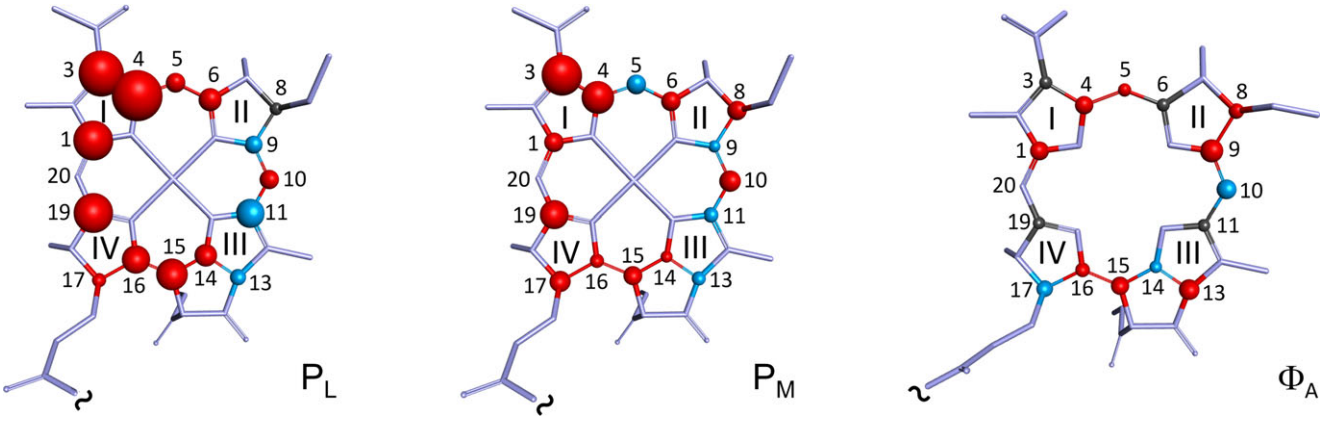

Figure 6. Difference in the relative electron densities of the electronic ground state, observed through the chemical shifts ($\Delta\sigma = \sigma_{ss}^{ph.-CIDNP} - \sigma_{liq}$) for the isotope-labeled sites (represented by spheres) in the cofactors involved into the formation of the spin-correlated radical pair (SCRP) (electron donor cofactors P_L and P_M and electron acceptor bacteriopheophytin Φ_A). Red spheres depicted the upfield shift or shielding, whereas the blue spheres indicate downfield shift or deshielding. The isotope-labeled positions showing negligible change (<0.3 ppm) are labeled by gray circles. The pyrrole rings are indicated by Roman numbers. The long side chains are omitted (at the position marked by ~) for better visual clarity.

Hence, the ground-state electronic symmetry is already broken (36). As reason for such symmetry break, not far-reaching Coulomb effects, no difference on the acceptor site (35) but local effects from side-chain folding (39,41,85,87) and assumable particular macrocycle foldings (88) are responsible. On the primary electron acceptor cofactor, both upfield and downfield shifts of a negligible magnitude ($\Delta\sigma < 2.6$) imply an electronic structure similar to that of a free bacteriopheophytin is acetone (35).

CONCLUSIONS

The application of a 2D homonuclear DQ-SQ POST-C7 recoupling scheme under continuous illumination and MAS NMR has been presented for the signal assignment of a selectively isotope-labeled RCs of *R. sphaeroides* WT. This dipolar INADEQUATE type requires much shorter experimental time for establishing and resolving all single-bond correlations compared to standard homonuclear correlation techniques (RFDR, DARR, etc.) because only one spectrum is required to reveal all connectivities in the molecule instead of multiple ones with different mixing times. Furthermore, this approach also yields less crowded spectra free of the influence of photo-induced isolated spins. This method will be applied to other known and newly discovered photosynthetic RCs. The method will allow to straightforwardly determine the number of cofactors involved into the formation of the SCRP and its electronic symmetry.

Applying this new approach, we achieved to separate the light-induced signals from the cofactors forming the SCRP, and even frequencies close to each other were distinguished. Thus, several of resonances from the P_L and P_M donor and the Φ_A acceptor have been reassigned. We conclusively established that light-induced signals occur only from three but not from four cofactors. Concerning the Special Pair, it is partially negatively charged, carries the surplus on negative charge in the overlapping region and has more electron density on P_L than on P_M. These construction features appear to be inspiriting for reconstruction in artificial photosynthesis.

Acknowledgements—M. Najdanova wishes to acknowledge the German Academic Exchange Service (DAAD) for a research fellowship. D. Gräsing thanks the Fonds der Chemischen Industrie for the granted scholarship. This work has been supported in part by a DFG Grant (MA 4972/2-1). The authors thank Prof. P.K. Madhu for discussions. Technical support from Dr. Chen Song, Pavlo Bielytskyi and Dr. Matthias Findeisen is gratefully acknowledged.

SUPPORTING INFORMATION

Additional Supporting Information may be found in the online version of this article:

Figure S1. 1D ^{13}C MAS DQ-SQ POST C7 spectrum of [5-^{13}C]-*δ*-aminolevulinic acid RC of *Rhodobacter sphaeroides* WT in the dark.

Figure S2. Full 2D ^{13}C photo-CIDNP MAS SQ-DQ photo-CIDNP ^{13}C-^{13}C correlation MAS NMR spectrum of selectively labeled [$^{13}C_{0\text{-}8}$] BChl/BPhe-labeled RCs from *Rhodobacter sphaeroides* WT under continuous illumination with white light, at a magnetic field strength of 9.4 T, temperature of 254 K, spinning frequency of 8 kHz.

Table S1. Summary of ^{13}C (SQ) and (DQ) chemical shifts assignment of the photo-CIDNP signals from BRC of *Rhodobacter sphaeroides* WT obtained at 9.4 T.

REFERENCES

1. Blankenship, R. E. (2014) *Molecular Mechanisms of Photosynthesis*, 2nd edn. Wiley-Blackwell, Oxford, UK.
2. Kê, B. (2001) *Photosynthesis Photobiochemistry and photobiophysics*. Kluwer Academic Publishers, Dordrecht, Boston, MA.
3. Hoff, A. J. and J. Deisenhofer (1997) Photophysics of photosynthesis. Structure and spectroscopy of reaction centers of purple bacteria. *Phys. Rep.* **287**, 1–247.
4. Blankenship, R. E., M. T. Madigan and C. E. Bauer (2006) *Anoxygenic Photosynthetic Bacteria*. Kluwer Academic Publishers, Dordrecht, The Netherlands.
5. Camara-Artigas, A., C. Magee, A. Goetsch and J. P. Allen (2002) The structure of the heterodimer reaction center from *Rhodobacter sphaeroides* at 2.55 å resolution. *Photosynth. Res.* **74**, 87–93.
6. Deisenhofer, J., O. Epp, K. Miki, R. Huber and H. Michel (1984) X-ray structure analysis of a membrane protein complex. Electron density map at 3 A resolution and a model of the chromophores of the photosynthetic reaction center from Rhodopseudomonas viridis. *J. Mol. Biol.* **180**, 385–398.
7. Williams, J. C. and J. P. Allen (2009) Directed modification of reaction centers from purple bacteria. In *The Purple Phototrophic Bacteria* Vol. 28 (Edited by C. N. Hunter, F. Daldal, M. C. Thurnauer and J. T. Beatty), pp. 337–353. Springer, Dordrecht, The Netherlands.
8. Holzwarth, A. R., M. G. Müller, J. Niklas and W. Lubitz (2006) Ultrafast transient absorption studies on photosystem I reaction centers from *Chlamydomonas reinhardtii*. 2: mutations near the P700 reaction center chlorophylls provide new insight into the nature of the primary electron donor. *Biophys. J.* **90**, 552–565.
9. Käss, H., P. Fromme, H. T. Witt and W. Lubitz (2001) Orientation and electronic structure of the primary donor radical cation in photosystem I: a single crystals EPR and ENDOR Study. *J. Phys. Chem. B* **105**, 1225–1239.
10. Sun, C., A.-M. Carey, B.-R. Gao, C. A. Wraight, N. W. Woodbury and S. Lin (2016) Ultrafast electron transfer kinetics in the LM dimer of bacterial photosynthetic reaction center from *Rhodobacter sphaeroides*. *J. Phys. Chem. B* **120**, 5395–5404.
11. Dahlberg, P. D., P.-C. Ting, S. C. Massey, E. C. Martin, C. N. Hunter and G. S. Engel (2016) Electronic structure and dynamics of higher-lying excited states in light harvesting complex 1 from *Rhodobacter sphaeroides*. *J. Phys. Chem. A* **120**, 4124–4130.
12. Marchanka, A., A. Savitsky, W. Lubitz, K. Möbius and M. van Gastel (2010) B-branch electron transfer in the photosynthetic reaction center of a *Rhodobacter sphaeroides* quadruple mutant. Q- and W-band electron paramagnetic resonance studies of triplet and radical-pair cofactor states †. *J. Phys. Chem. B* **114**, 14364–14372.
13. Eisenmayer, T. J., J. A. Lasave, A. Monti, H. J. M. de Groot and F. Buda (2013) Proton displacements coupled to primary electron transfer in the *Rhodobacter sphaeroides* reaction center. *J. Phys. Chem. B* **117**, 11162–11168.
14. Wang, H., Y. Hao, Y. Jiang, S. Lin and N. W. Woodbury (2012) Role of protein dynamics in guiding electron-transfer pathways in reaction centers from *Rhodobacter sphaeroides*. *J. Phys. Chem. B* **116**, 711–717.
15. Hunter, C. N., F. Daldal, M. C. Thurnauer and J. T. Beatty, eds. (2009) *The Purple Phototrophic Bacteria*. Springer, Dordrecht, The Netherlands.
16. Holzwarth, A. R. and M. G. Müller (1996) Energetics and kinetics of radical pairs in reaction centers from *Rhodobacter sphaeroides*. A femtosecond transient absorption study†,‡. *Biochemistry* **35**, 11820–11831.
17. Scheer, H. (ed.) (1991) *Chlorophylls*. CRC Press, Boca Raton, FL.
18. Jeschke, G., B. C. Anger, B. E. Bode and J. Matysik (2011) Theory of solid-state photo-CIDNP in the Earth's magnetic field. *J. Phys. Chem. A* **115**, 9919–9928.

19. Daviso, E. (2008) The solid-state photo-CIDNP effect. PhD thesis, Leiden, The Netherlands.
20. Daviso, E., A. Alia, S. Prakash, A. Diller, P. Gast, J. Lugtenburg, J. Matysik and G. Jeschke (2009) Electron−nuclear spin dynamics in a bacterial photosynthetic reaction center. *J. Phys. Chem. C* **113**, 10269–10278.
21. Thamarath, S. S., B. E. Bode, S. Prakash, K. B. Sai Sankar Gupta, A. Alia, G. Jeschke and J. Matysik (2012) Electron spin density distribution in the special pair triplet of *Rhodobacter sphaeroides* R26 revealed by magnetic field dependence of the solid-state photo-CIDNP effect. *J. Am. Chem. Soc.* **134**, 5921–5930.
22. Jeschke, G. (1997) Electron–electron–nuclear three-spin mixing in spin-correlated radical pairs. *J. Chem. Phys.* **106**, 10072–10086.
23. Polenova, T. and A. E. McDermott (1999) A coherent mixing mechanism explains the photoinduced nuclear polarization in photosynthetic reaction centers †. *J. Phys. Chem. B* **103**, 535–548.
24. Kaptein, R. and J. L. Oosterhoff (1969) Chemically induced dynamic nuclear polarization II. *Chem. Phys. Lett.* **4**, 195–197.
25. Closs, G. L. and L. E. Closs (1969) Induced dynamic nuclear spin polarization in photoreductions of benzophenone by toluene and ethylbenzene. *J. Am. Chem. Soc.* **91**, 4550–4552.
26. Zysmilich, M. G. and A. McDermott (1994) Photochemically induced dynamic nuclear polarization in the solid-state 15N spectra of reaction centers from photosynthetic bacteria *Rhodobacter sphaeroides* R-26. *J. Am. Chem. Soc.* **116**, 8362–8363.
27. Matysik, J., P. Gast, H. J. van Gorkom, A. J. Hoff and H. J. M. de Groot (2000) Photochemically induced nuclear spin polarization in reaction centers of photosystem II observed by 13C-solid-state NMR reveals a strongly asymmetric electronic structure of the P680.+ primary donor chlorophyll. *Proc. Natl Acad. Sci. USA* **97**, 9865–9870.
28. Matysik, J., A. Alia, J. G. Hollander, T. Egorova-Zachernyuk, P. Gast and H. J. de Groot (2000) A set-up to study photochemically induced dynamic nuclear polarization in photosynthetic reaction centres by solid-state NMR. *Indian J. Biochem. Biophys.* **37**, 418–423.
29. Bode, B. E., S. S. Thamarath, K. B. S. S. Gupta, A. Alia, G. Jeschke and J. Matysik (2013) The solid-state photo-CIDNP effect and its analytical application. In *Hyperpolarization Methods in NMR Spectroscopy* Vol. 338. (Edited by L. T. Kuhn), pp. 105–121. Springer, Berlin Heidelberg.
30. Céspedes-Camacho, I. F. and J. Matysik (2014) Spin in photosynthetic electron transport. In *The Biophysics of Photosynthesis* (Edited by J. Golbeck and van der Est A.), pp. 141–170. Springer, New York.
31. Najdanova, M., G. J. Janssen, H. de Groot, J. Matysik and A. Alia (2015) Analysis of electron donors in photosystems in oxygenic photosynthesis by photo-CIDNP MAS NMR. *J. Photochem. Photobiol., B* **152**, 261–271.
32. Zill, J. C., M. Kansy, R. Goss, L. Köhler, A. Alia, C. Wilhelm and J. Matysik (2017) Photo-CIDNP in the reaction center of the diatom *Cyclotella meneghiniana* observed by 13C MAS NMR. *Z. Phys. Chem.* **231**, 347–367.
33. Matysik, J., A. Diller, E. Roy and A. Alia (2009) The solid-state photo-CIDNP effect. *Photosynth. Res.* **102**, 427–435.
34. Surendran Thamarath, S., A. Alia, E. Roy, K. B. Sai Sankar Gupta, J. H. Golbeck and J. Matysik (2013) The field-dependence of the solid-state photo-CIDNP effect in two states of heliobacterial reaction centers. *Photosynth. Res.* **117**, 461–469.
35. Sai Sankar Gupta, K. B., A. Alia, F. Buda, H. J. M. de Grootand J. Matysik (2013) Bacteriopheophytin a in the active branch of the reaction center of *Rhodobacter sphaeroides* is not disturbed by the protein matrix as shown by 13 C photo-CIDNP MAS NMR. *J. Phys. Chem. B* **117**, 3287–3297.
36. Schulten Els, A. M., J. Matysik, S. Alia, J. Kiihne, J. Raap, P. Lugtenburg, A. J. Hoff Gast and H. J. M. de Groot (2002) 13 C MAS NMR and photo-CIDNP reveal a pronounced asymmetry in the electronic ground state of the special pair of *Rhodobacter sphaeroides* reaction centers †. *Biochemistry* **41**, 8708–8717.
37. Prakash, S., A. Alia, P. Gast, H. J. M. de Groot, G. Jeschke and J. Matysik (2007) 13 C chemical shift map of the active cofactors in photosynthetic reaction centers of *Rhodobacter sphaeroides* revealed by photo-CIDNP MAS NMR †. *Biochemistry* **46**, 8953–8960.
38. Daviso, E., S. Prakash, A. Alia, P. Gast, J. Neugebauer, G. Jeschke and J. Matysik (2009) The electronic structure of the primary electron donor of reaction centers of purple bacteria at atomic resolution as observed by photo-CIDNP 13C NMR. *Proc. Natl Acad. Sci. USA* **106**, 22281–22286.
39. Lendzian, F., M. Huber, R. A. Isaacson, B. Endeward, M. Plato, B. Bönigk, K. Möbius, W. Lubitz and G. Feher (1993) The electronic structure of the primary donor cation radical in *Rhodobacter sphaeroides* R-26: ENDOR and TRIPLE resonance studies in single crystals of reaction centers. *Biochim. Biophys. Acta* **1183**, 139–160.
40. Alia, A., P. K. Wawrzyniak, G. J. Janssen, F. Buda, J. Matysik and H. J. M. de Groot (2009) Differential charge polarization of axial histidines in bacterial reaction centers balances the asymmetry of the special pair. *J. Am. Chem. Soc.* **131**, 9626–9627.
41. Sai Sankar Gupta, K. B., A. Alia, H. J. M. de Groot and J. Matysik (2013) Symmetry break of special pair: photochemically induced dynamic nuclear polarization NMR confirms control by nonaromatic substituents. *J. Am. Chem. Soc.* **135**, 10382–10387.
42. Bennett, A. E., R. G. Griffin, J. H. Ok and S. Vega (1992) Chemical shift correlation spectroscopy in rotating solids: Radio frequency-driven dipolar recoupling and longitudinal exchange. *J. Chem. Phys.* **96**, 8624–8627.
43. Ishii, Y. (2001) 13C–13C dipolar recoupling under very fast magic angle spinning in solid-state nuclear magnetic resonance: applications to distance measurements, spectral assignments, and high-throughput secondary-structure determination. *J. Chem. Phys.* **114**, 8473–8483.
44. Bennett, A. E., C. M. Rienstra, M. Auger, K. V. Lakshmi and R. G. Griffin (1995) Heteronuclear decoupling in rotating solids. *J. Chem. Phys.* **103**, 6951–6958.
45. Sai Sankar Gupta, K. B., E. Daviso, G. Jeschke, A. Alia, M. Ernst and J. Matysik (2014) Spectral editing through laser-flash excitation in two-dimensional photo-CIDNP MAS NMR experiments. *J. Magn. Reson.* **246**, 9–17.
46. Paul, S., B. E. Bode, J. Matysik and A. Alia (2015) Photochemically induced dynamic nuclear polarization observed by solid-state NMR in a uniformly 13 C-isotope-labeled photosynthetic reaction center. *J. Phys. Chem. B* **119**, 13897–13903.
47. Bax, A., R. Freeman and S. P. Kempsell (1980) Natural abundance carbon-13-carbon-13 coupling observed via double-quantum coherence. *J. Am. Chem. Soc.* **102**, 4849–4851.
48. Bax, A., R. Freeman and T. A. Frenkiel (1981) An NMR technique for tracing out the carbon skeleton of an organic molecule. *J. Am. Chem. Soc.* **103**, 2102–2104.
49. Bax, A., R. Freeman, T. Frenkiel and M. Levitt (1981) Assignment of carbon-13 NMR spectra via double-quantum coherence. *J. Magn. Reson.* **43**, 478–483.
50. Lee, Y., N. Kurur, M. Helmle, O. Johannessen, N. Nielsen and M. Levitt (1995) Efficient dipolar recoupling in the NMR of rotating solids. A sevenfold symmetric radiofrequency pulse sequence. *Chem. Phys. Lett.* **242**, 304–309.
51. Hohwy, M., H. J. Jakobsen, M. Edén, M. H. Levitt and N. C. Nielsen (1998) Broadband dipolar recoupling in the nuclear magnetic resonance of rotating solids: a compensated C7 pulse sequence. *J. Chem. Phys.* **108**, 2686–2694.
52. Hong, M. (1999) Solid-state dipolar INADEQUATE NMR spectroscopy with a large double-quantum spectral width. *J. Magn. Reson.* **136**, 86–91.
53. Nielsen, N. C., H. Bildso/e, H. J. Jakobsen and M. H. Levitt (1994) Double-quantum homonuclear rotary resonance: efficient dipolar recovery in magic-angle spinning nuclear magnetic resonance. *J. Chem. Phys.* **101**, 1805–1812.
54. Kristiansen, P. E., D. J. Mitchell and J. N. Evans (2002) Double-quantum dipolar recoupling at high magic-angle spinning rates. *J. Magn. Reson.* **157**, 253–266.
55. Kristiansen, P. E., M. Carravetta, W. C. Lai and M. H. Levitt (2004) A robust pulse sequence for the determination of small homonuclear dipolar couplings in magic-angle spinning NMR. *Chem. Phys. Lett.* **390**, 1–7.
56. Kristiansen, P. E., M. Carravetta, J. D. van Beek, W. C. Lai and M. H. Levitt (2006) Theory and applications of supercycled symmetry-based recoupling sequences in solid-state nuclear magnetic resonance. *J. Chem. Phys.* **124**, 234510.
57. Levitt, M. H. (2007) Symmetry-based pulse sequences in magic-angle spinning solid-state NMR. In *Encyclopedia of Magnetic Resonance* (Edited by R. K. Harris and R. Wasylishen). John Wiley & Sons LTD, Chichester, UK.

58. Lee, M. and W. I. Goldburg (1965) Nuclear-magnetic-resonance line narrowing by a rotating rf field. *Phys. Rev.* **140**, A1261.
59. Brinkmann, A., M. Edén and M. H. Levitt (2000) Synchronous helical pulse sequences in magic-angle spinning nuclear magnetic resonance: double quantum recoupling of multiple-spin systems. *J. Chem. Phys.* **112**, 8539–8554.
60. Shochat, S., T. Arlt, C. Francke, P. Gast, P. I. van Noort, S. C. M. Otte, H. P. M. Schelvis, S. Schmidt, E. Vijgenboom, J. Vrieze, W. Zinth and A. J. Hoff (1994) Spectroscopic characterization of reaction centers of the (M)Y210W mutant of the photosynthetic bacterium *Rhodobacter sphaeroides*. *Photosynth. Res.* **40**, 55–66.
61. Okamura, M. Y., R. A. Isaacson and G. Feher (1975) Primary acceptor in bacterial photosynthesis: obligatory role of ubiquinone in photoactive reaction centers of *Rhodopseudomonas spheroides*. *Proc. Natl Acad. Sci. USA* **72**, 3491–3495.
62. Fischer, M. R., H. J. M. de Groot, J. Raap, C. Winkel, A. J. Hoff and J. Lugtenburg (1992) Carbon-13 magic angle spinning NMR study of the light-induced and temperature-dependent changes in *Rhodobacter sphaeroides* R26 reaction centers enriched in [4′-13C] tyrosine. *Biochemistry* **31**, 11038–11049.
63. Ramamoorthy, A. (Sept. 2005) *NMR Spectroscopy of Biological Solids*. C R C Press LLC, Taylor & Francis Group [distributor], Boca Raton, Florence.
64. Thurber, K. R. and R. Tycko (2008) Biomolecular solid state NMR with magic-angle spinning at 25K. *J. Magn. Reson.* **195**, 179–186.
65. Chow, W. Y., R. Rajan, K. H. Muller, D. G. Reid, J. N. Skepper, W. C. Wong, R. A. Brooks, M. Green, D. Bihan, R. W. Farndale, D. A. Slatter, C. M. Shanahan and M. J. Duer (2014) NMR spectroscopy of native and *in vitro* tissues implicates PolyADP ribose in biomineralization. *Science* **344**, 742–746.
66. Pahari, B., N. Mhadhbi, G. Corbel, P. Lacorre and J. Dittmer (2012) Analysis of the local structure of phosphorus-substituted LAMOX oxide ion conductors. *Dalton Trans.* **41**, 5696.
67. Ladizhansky, V. and S. Vega (2000) Polarization transfer dynamics in Lee-Goldburg cross polarization nuclear magnetic resonance experiments on rotating solids. *J. Chem. Phys.* **112**, 7158–7168.
68. Fung, B. M., A. K. Khitrin and K. Ermolaev (2000) An improved broadband decoupling sequence for liquid crystals and solids. *J. Magn. Reson.* **142**, 97–101.
69. Comellas, G., J. J. Lopez, A. J. Nieuwkoop, L. R. Lemkau and C. M. Rienstra (2011) Straightforward, effective calibration of SPINAL-64 decoupling results in the enhancement of sensitivity and resolution of biomolecular solid-state NMR. *J. Magn. Reson.* **209**, 131–135.
70. Takegoshi, K., S. Nakamura and T. Terao (2001) 13C–1H dipolar-assisted rotational resonance in magic-angle spinning NMR. *Chem. Phys. Lett.* **344**, 631–637.
71. Nielsen, N. C., F. Creuzet, R. G. Griffin and M. H. Levitt (1992) Enhanced double-quantum nuclear magnetic resonance in spinning solids at rotational resonance. *J. Chem. Phys.* **96**, 5668–5677.
72. Lesage, A., C. Auger, S. Caldarelli and L. Emsley (1997) Determination of through-bond carbon−carbon connectivities in solid-state NMR using the INADEQUATE experiment. *J. Am. Chem. Soc.* **119**, 7867–7868.
73. Menger, E. M., S. Vega and R. G. Griffin (1986) Observation of carbon-carbon connectivities in rotating solids. *J. Am. Chem. Soc.* **108**, 2215–2218.
74. Ernst, M., M. A. Meier, T. Tuherm, A. Samoson and B. H. Meier (2004) Low-power high-resolution solid-state NMR of peptides and proteins. *J. Am. Chem. Soc.* **126**, 4764–4765.
75. Baldus, M. and B. H. Meier (1997) Broadband polarization transfer under magic-angle spinning: application to total through-space-correlation NMR spectroscopy. *J. Magn. Reson.* **128**, 172–193.
76. Prakash, S., P. Gast Alia, H. J. M. de Groot, G. Jeschke and J. Matysik (2005) Magnetic field dependence of photo-CIDNP MAS NMR on photosynthetic reaction centers of *Rhodobacter sphaeroides* WT. *J. Am. Chem. Soc.* **127**, 14290–14298.
77. Jeschke, G. and J. Matysik (2003) A reassessment of the origin of photochemically induced dynamic nuclear polarization effects in solids. *Chem. Phys.* **294**, 239–255.
78. Abraham, R. J. and A. E. Rowan (1991) Nuclear magnetic resonance spectroscopy of Chlorophyll. In *Chlorophylls* (Edited by H. Scheer), pp. 797–834. CRC Press, Boca Raton, FL.
79. Abraham, R. J., A. E. Rowan, N. W. Smith and K. M. Smith (1993) NMR spectra of the porphyrins. Part 42. The synthesis and aggregation behaviour of some chlorophyll analogues. *J. Chem. Soc., Perkin Trans. 1* **2**, 1047–1059.
80. Egorova-Zachernyuk, T., B. van Rossum, C. Erkelens and H. de Groot (2008) Characterisation of uniformly 13C, 15N labelled bacteriochlorophyll a and bacteriopheophytin a in solution and in solid state: complete assignment of the 13C, 1H and 15N chemical shifts. *Magn. Reson. Chem.* **46**, 1074–1083.
81. Daviso, E., S. Prakash, A. Alia, P. Gast, G. Jeschke and J. Matysik (2010) Nanosecond-flash 15N photo-CIDNP MAS NMR on reaction centers of *Rhodobacter sphaeroides* R26. *Appl. Magn. Reson.* **37**, 49–63.
82. Vanderhart, D., W. L. Earl and A. Garroway (1981) Resolution in 13C NMR of organic solids using high-power proton decoupling and magic-angle sample spinning. *J. Magn. Reson.* **44**, 361–401.
83. Hodgkinson, P. (2005) Heteronuclear decoupling in the NMR of solids. *Prog. Nucl. Magn. Reson. Spectrosc.* **46**, 197–222.
84. Wawrzyniak, P. K., M. T. P. Beerepoot, H. J. M. de Groot and F. Buda (2011) Acetyl group orientation modulates the electronic ground-state asymmetry of the special pair in purple bacterial reaction centers. *Phys. Chem. Chem. Phys.* **13**, 10270.
85. Yamasaki, H., Y. Takano and H. Nakamura (2008) Theoretical investigation of the electronic asymmetry of the special pair cation radical in the photosynthetic type-II reaction center. *J. Phys. Chem. B* **112**, 13923–13933.
86. Plato, M., F. Lendzian, W. Lubitz and K. Möbius (1992) Molecular orbital study of electronic asymmetry in primary donors of bacterial reaction centers. In *The Photosynthetic Bacterial Reaction Center II* (Edited by J. Breton and A. Verméglio), pp. 109–118. Springer, Boston, MA.
87. Rautter, J., F. Lendzian, W. Lubitz, S. Wang and J. P. Allen (1994) Comparative study of reaction centers from photosynthetic purple bacteria: electron paramagnetic resonance and electron nuclear double resonance spectroscopy. *Biochemistry* **33**, 12077–12084.
88. Senge, M., A. Ryan, K. Letchford, S. MacGowan and T. Mielke (2014) Chlorophylls, symmetry, chirality, and photosynthesis. *Symmetry* **6**, 781–843.
89. Grimm, B. (2006) *Chlorophylls and Bacteriochlorophylls. Biochemistry, Biophysics, Functions and Applications*. Springer, Dordrecht, The Netherlands.
90. Mamedov, M., V. N. Govindjee and A. Semenov (2015) Primary electron transfer processes in photosynthetic reaction centers from oxygenic organisms. *Photosynth. Res.* **125**, 51–63.